Environmental Science & Technology

pubs.acs.org/est

Article

Characterization of Atmospheric Processes of Brevetoxins in Sea Spray Aerosols from Red Tide Events

Karen Sem, Myoseon Jang,* Richard Pierce, Patricia Blum, and Zechen Yu

Cite This: *Environ. Sci. Technol.* 2022, 56, 1811−1819

Read Online

ACCESS | Metrics & More | Article Recommendations | Supporting Information

ABSTRACT: Atmospheric processes can affect the longevity of harmful toxins in sea spray aerosols (SSA). This study characterized the degradation of brevetoxin (BTx) in SSA under different environmental conditions. The samples of seawater collected during a *Karenia brevis* bloom in Manasota, Florida, were nebulized into a large outdoor photochemical chamber to mimic the atmospheric oxidation of aerosolized toxins and then aged in the presence or absence of sunlight and/or O_3. Aerosol samples were collected during the aging process using a Particle-Into-Liquid Sampler. Their BTx concentrations were measured using an enzyme-linked immuno-sorbent assay (ELISA) and high-performance liquid chromatography/tandem mass spectroscopy. The BTx ozonolysis rate constant measured by ELISA was 5.74 ± 0.21 × 10^3 M^{-1} s^{-1}. The corresponding lifetime for decay of 87.5% BTx in the presence of 20 ppb of O_3 was 7.08 ± 0.26 h, suggesting that aerosolized BTx can still travel long distances at night before SSA deposition. BTx concentrations in SSA decreased more rapidly in the presence of sunlight than in its absence due to oxidation with photochemically produced OH radicals.

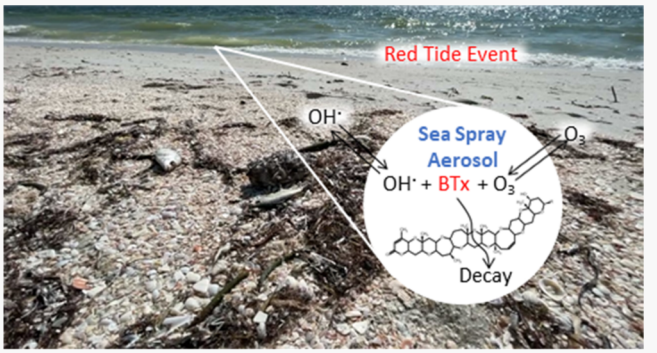

KEYWORDS: *harmful algal blooms, brevetoxin, sea spray aerosol, atmospheric oxidation, algal aerosol*

INTRODUCTION

Karenia brevis is a dinoflagellate native to the waters of the Gulf of Mexico and the Caribbean. It forms the primary component of harmful algae blooms known as "red tide," which recur in its native regions and spread to neighboring coastlines during the late summer and fall.[1] The species produces a polyether neurotoxin known as brevetoxin (BTx), which is then released into surrounding waters via excretion and cell rupture.[2] When ingested, BTx displays an antagonistic effect on neurons by binding to receptors on voltage-gated sodium channels, which can result in severe gastrointestinal and neurological symptoms.[3,4]

Excreted BTx can also be incorporated into sea spray aerosols (SSA), particles formed from the bursting of bubbles at the ocean's surface.[2] When inhaled at concentrations greater than 3−4 ng/m^3, BTx can induce cough, shortness of breath, and other symptoms in the upper and lower respiratory tracts.[4−6] Atmospheric concentrations of BTx in coastal SSA can exceed this level by approximately 1 order of magnitude during red tide events.[6,7] For example, SSA collected during a red tide event on Siesta Key on the Florida Gulf Coast contained BTx-2 + 3 concentrations of 35 ng/m^3 in the morning and 25 ng/m^3 in the afternoon.[7] Concentrations of *K. brevis* in the surf ranged from 165,000 to 225,000 cells/L throughout the day, with onshore winds averaging 10 km/h.[7] Though a naturally occurring phenomenon, red tide events like the one at Siesta Key have increased in severity and length from the effects of local pollution and global climate change, as *K. brevis* growth is sustained by excess nutrients from agricultural, industrial, and urban runoff and by warmer ocean temperatures year round.[1] Exposure of aerosolized BTx to coastal communities through the transport of SSA generated from red tide events to nearby shores can result in significant economic impacts from increased hospitalizations and decreased tourism.[8]

BTx's molecular structure is characterized by a long polyether backbone with a single lactone group on a terminal ring and a side chain on the other.[9] Variants of BTx found during a red tide event may possess one of two different backbones found in the parent molecules, BTx A and BTx B (Figure 1). Derivatives of BTx can have various functions, ranging from increased neurotoxicity to antagonistic effects on parental BTx compounds.[9] BTx-2 and BTx-3 in the BTx B class are the most abundant toxins observed during blooms.[10−12] BTx-3 is the most abundant variant observed in

Received: August 27, 2021
Revised: December 2, 2021
Accepted: January 5, 2022
Published: January 20, 2022

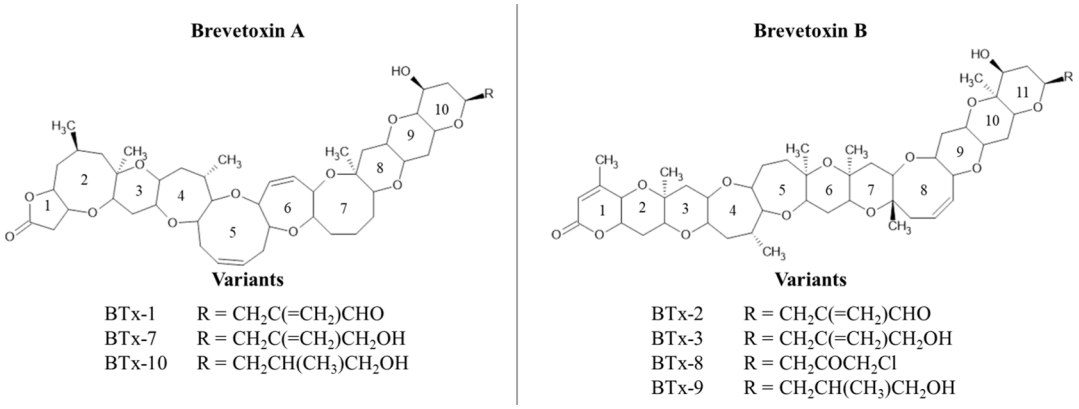

Figure 1. Structural backbones of BTx A and BTx B and R groups of variants.[9,12]

extracellular conditions due to its selection by the environmental conditions of bulk seawater.[10−12] Previous studies have demonstrated the ability of BTx to undergo transformation in seawater from photodegradation and ozonation.[13−15] However, the transformation of aerosolized BTx is currently unexplored. Recent studies have shown that the ADDA unit of aerosolized microcystin-LR in freshwater cyanobacteria can undergo degradation during atmospheric aging.[16] In a similar manner, double-bonded moieties in rings and side chains of aerosolized BTx may undergo transformation through heterogeneous reactions with atmospheric oxidants such as ozone (O_3) and hydroxyl (OH) radicals.

Characterization of the phase state of SSA is necessary for the identification of the reaction rate constants of BTx with atmospheric oxidants. The ocean surface consists of a thin film with a higher organic matter (OM) content than bulk seawater, though the composition and size of the OM fraction in the surface microlayer may vary based on bloom conditions.[17,18] This OM fraction is preserved in SSA formed from wind and wave motion, which consists of a salted aqueous core covered by an organic coating (Figure 2).[19−21] SSA form in the marine

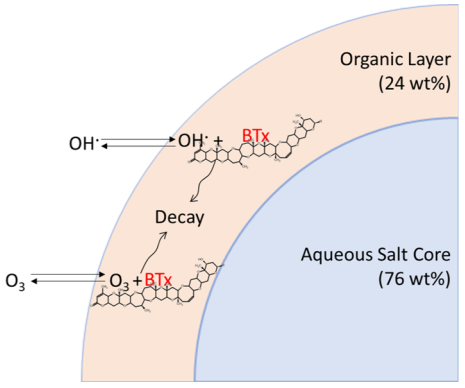

Figure 2. Atmospheric processes of aerosolized BTx on typical SSA.[26]

boundary layer, where they deliquesce at a relative humidity (RH) of 75.3%.[22] As SSA are carried inland by sea breezes, they lose mass through water evaporation until they effloresce at approximately 10.8% RH.[23] Phase separation between the organic and aqueous content of SSA begins at around 90−92% RH and is maintained as RH decreases.[24,25] The phase of SSA influences the rates of uptake and reaction of atmospheric oxidants with BTx.

This study investigated the factors that influence the lifetime of aerosolized BTx in various atmospheric environments. Authentic seawater collected during a red tide event was nebulized into the University of Florida's Atmospheric Photochemical Outdoor Reactor (UF-APHOR) dual chambers and atmospherically aged in the presence of O_3 or sunlight. The rate and extent of BTx decay were characterized by measuring its concentration in aerosol samples collected at various stages of the aging process using an enzyme-linked immuno-sorbent assay (ELISA) and liquid chromatography/tandem mass spectroscopy (LC/MS/MS). Using calculations from thermodynamic models based on group contributions,[27,28] BTx was assumed to be predominantly located in the organic layer of SSA. Consequently, the reaction rate constant of BTx with atmospheric oxidants was estimated based on this assumption. The impact of coexisting OM on the rate and extent of BTx decay in SSA was also studied. Greater knowledge of the factors that influence the decay of aerosolized BTx can be used to better understand and predict the impact of aerosolized red tide algae on nearby communities.

EXPERIMENTAL SECTION

Chamber Experiments. To study the degradation of aerosolized BTx under different atmospheric conditions, SSA containing BTx were introduced into the UF-APHOR dual chambers (volume = 52/52 m^3). Table 1 summarizes chamber experimental conditions. Seawater was collected from a red tide event in Manasota, Florida, on October 13, 2020, and stored at −20 °C to prevent BTx decay between collection and chamber experimentation. Prior to each experiment, 10 mL aliquots of seawater were sonicated for 10 min to lyse algal cells and diluted 10-fold to form an analogue of SSA containing BTx.

To observe the effects of the OM fraction found in SSA in Experiments H, J, K, and L in Table 1, a 9.26 mg spike of OM was added to 10 mL of the diluted solution to simulate the average composition of the OM fraction in SSA.[26] The spike consisted of α-D-glucose (96%, Sigma-Aldrich), stearic acid (Fisher Scientific), and bovine serum albumin (BSA) (Fraction V, Crystalline, Sigma-Aldrich) based on reported literature values.[26] These compounds were selected due to their possession of functional groups found frequently in the OM fraction of SSA. After preparation of the 10-fold diluted solution, it was divided into 3 mL aliquots. To observe the effects of photosensitizing OM on BTx transformation in Experiment L, 3 μL of a 0.53 wt % chlorophyll (Chl) solution

https://doi.org/10.1021/acs.est.1c05740
Environ. Sci. Technol. 2022, 56, 1811−1819

Table 1. Experimental Conditions of Atmospheric Oxidation Experiments Performed with Algal Aerosol in the UF-APHOR Chambers

exp.	date	aliquot	reaction	$[SSA]_0$[b] ($\mu g/m^3$)	$[OM]_0$[c] ($\mu g/m^3$)	$[O_3]$ (ppb)	sunlight (W/m^2)	temp (°C)	RH (%)	comments
A	2/20/2021	*K. brevis*[a]	O_3	2165.5	0.0	30	0	7−21	81−89	Figures 3 and S2
B	4/11/2021	*K. brevis*	O_3	3550	0.0	33	0	16−23	82−93	Figures 3 and S2
C	5/21/2021	*K. brevis* and OM spike[d]	O_3	2485	596.4	29	0	18−21	89−97	Figures 3 and S2
D	2/7/2021	*K. brevis*	sunlight	2591.5	0.0	0−4	0−12	19−22	79−94	Figures 4 and S1
E	2/21/2021	*K. brevis*	sunlight	1100.5	0.0	0−5	0−13	5−27	57−96	Figures 4 and S1
F	4/5/2021	*K. brevis* and BTx−3 spike[e]	sunlight	5467	0.0	0−10	0−22	9−31	34−93	Figures 4 and S1
G	4/30/2021	*K. brevis*	sunlight	2165.5	0.0	0−21	0−35	19−46	23−87	Figures 5, S1 and S5
H	4/30/2021	*K. brevis* and OM spike	sunlight	3585.5	860.5	0−23	0−35	19−43	32−93	Figures 5, S1 and S5
I	7/30/2021	*K. brevis*	sunlight	1633	0.0	0−69	0−36	24−46	45−100	Figures 5 and S1
J	7/30/2021	*K. brevis* and OM spike	sunlight	319.5	76.7	0−66	0−36	24−46	32−96	Figures 5 and S1
K	7/27/2021	*K. brevis* and OM spike	sunlight	994	238.6	0−22	0−30	24−48	29−95	Figures 5 and S1
L	7/27/2021	*K. brevis* and OM/Chl spike[f]	sunlight	1029.5	247.1	0−24	0−30	24−45	41−99	Figures 5 and S1

[a]*K. brevis* sampled from red tide event at Manasota, Florida, on October 13, 2020. [b]$[SSA]_0$ is the initial dry mass concentration estimated by using SMPS data, the density of aerosol, and aerosol water content at the corresponding RH and temperature. The aerosol water content (AWC) was calculated using a regression equation estimated from data in literature:[29] $AWC = 0.5932e^{0.0041RH}$. $[SSA]_0$ was calculated using the equation $[SSA]_0 = \rho_{SSA}V_t(1 - AWC)$, where ρ_{SSA} is the reported density of dry sea salts (35.5 $\mu g/m^3$) and V_t is the volumetric concentration measured by SMPS. [c]$[OM]_0 = 0.24 \times [SSA]_0$ when OM spike is added. [d]OM spike contains 72% glucose, 23% BSA, and 5% stearic acid by weight.[26] [e]BTx-3 spike consists of 10 μL of 0.5 mg/mL solution in acetonitrile. [f]Chl spike is 3 μL of 0.53 wt % solution in water.

(World Organic) was added to the aliquot. For the observation of BTx transformation using LC/MS/MS in Experiment H (Table 1), 10 μL of an external 0.5 mg/mL BTx-3 spike (BTx PbTx-3, *Ptychodiscus brevis*, Sigma-Aldrich) was added to the aliquot so that the BTx concentration exceeded the instrument's detection limit.

In Experiments A−C (Table 1), O_3 was introduced into the chamber using an ozone generator (Teledyne, Waterzone 5000, Thousand Oaks, CA). Then, 3 mL aliquots of the 10-fold seawater dilution were nebulized into the UF-APHOR dual chambers (V = 52/52 m^3) in dark conditions to avoid photochemical reactions. For all experiments, 200−400 μL of CCl_4 (Thermo Fisher Scientific) was added to observe chamber dilution.

Chamber conditions were monitored over the course of the experiment by various instruments. Figure S1 shows the time profiles of chamber conditions for Experiments D−L, which were conducted in the presence of sunlight. Particle number concentration and population were measured by a Scanning Mobility Particle Sizer (TSI, model 3080, Shoreview, MN). The mass concentration of non-refractory particle fractions was measured by an Aerosol Chemical Speciation Monitor (Aerodyne, Billerica, MA). The geometric mean diameter of the generated aerosol ranged between 200 and 250 nm and the geometric standard deviation ranged between 15 and 17 nm. The mass concentrations of ions in aerosol samples were measured using an Ion Chromatograph coupled to a Particle-Into-Liquid Sampler (PILS) (Metrohm, Herisau, Switzerland). O_3 and NO_x concentrations were measured using a Photometric Ozone Analyzer (Teledyne, model 400E, Thousand Oaks, CA) and Chemiluminescence NO/NO_2 analyzer (Teledyne, model 200E, Thousand Oaks, CA), respectively. Temperature and RH within each chamber were measured using a Measurement and Control System (Campbell Scientific, model CR1000, Logan, UT). Solar UV radiation in each chamber was measured using a Total Ultraviolet Radiometer (Eppley Laboratory, Inc., Newport, RI). The organic carbon (OC) content in chamber-generated SSA was measured by using an OC Analyzer (Sunset Laboratories, model 4, Hillsborough, NC). The OC content in SSA of this study was 0.7 wt % of dry SSA. The UV spectra of aerosol particles collected on Teflon-coated glass fibers were measured using a micro-UV spectrometer (Ocean Optics, Dunedin, FL).

Aerosol Collection and BTx Analysis. Aerosol samples were taken using PILS (Metrohm, Herisau, Switzerland), which collected aerosol at an air flow rate of 14−15 L/min. The concentrations of particles in the collected samples were calculated using the gas and liquid flow rates of the PILS, SMPS data, and the aerosol density. The BTx concentration in each sample was measured in triplicates using an ELISA kit (Eurofins Analytics, Warminster, PA), which selected for BTx-B variants. For ELISA analysis, samples were spiked to contain 0.1% Tween 20 (Thermo Fisher Scientific) to prevent loss of BTx to vial surfaces and then stored at 4 °C. All samples were analyzed using ELISA within 6 h of sample collection. The reaction rate constants for BTx ozonolysis were calculated on the assumption that ozonolysis occurs in a pseudo-first-order reaction. The significant difference between rate constants for ozonolysis under different conditions was evaluated using the Student *t*-test. The reaction rate constants for BTx photolysis were not estimated due to the contribution of multiple oxidants to the reaction.

In Experiment F, BTx concentrations were measured using both LC/MS/MS and ELISA to evaluate the accuracy of the latter method in measuring BTx concentrations in aerosol. For LC/MS/MS analysis, 300 μL aliquots of the PILS sample were added to 1.2 mL methanol in the absence of Tween 20 and stored at −20 °C. BTx analysis was performed using the Thermo Electron Quantum Access LC/MS/MS system (Thermo Fisher Scientific, Waltham, MA). The LC consists of an Accela UHPLC pumping system (Thermo Fisher Scientific, Waltham, MA), coupled with the Accela Autosampler and Degasser (Thermo Fisher Scientific, Waltham, MA). Mass spectral detection was obtained using the Quantum

https://doi.org/10.1021/acs.est.1c05740
Environ. Sci. Technol. 2022, 56, 1811−1819

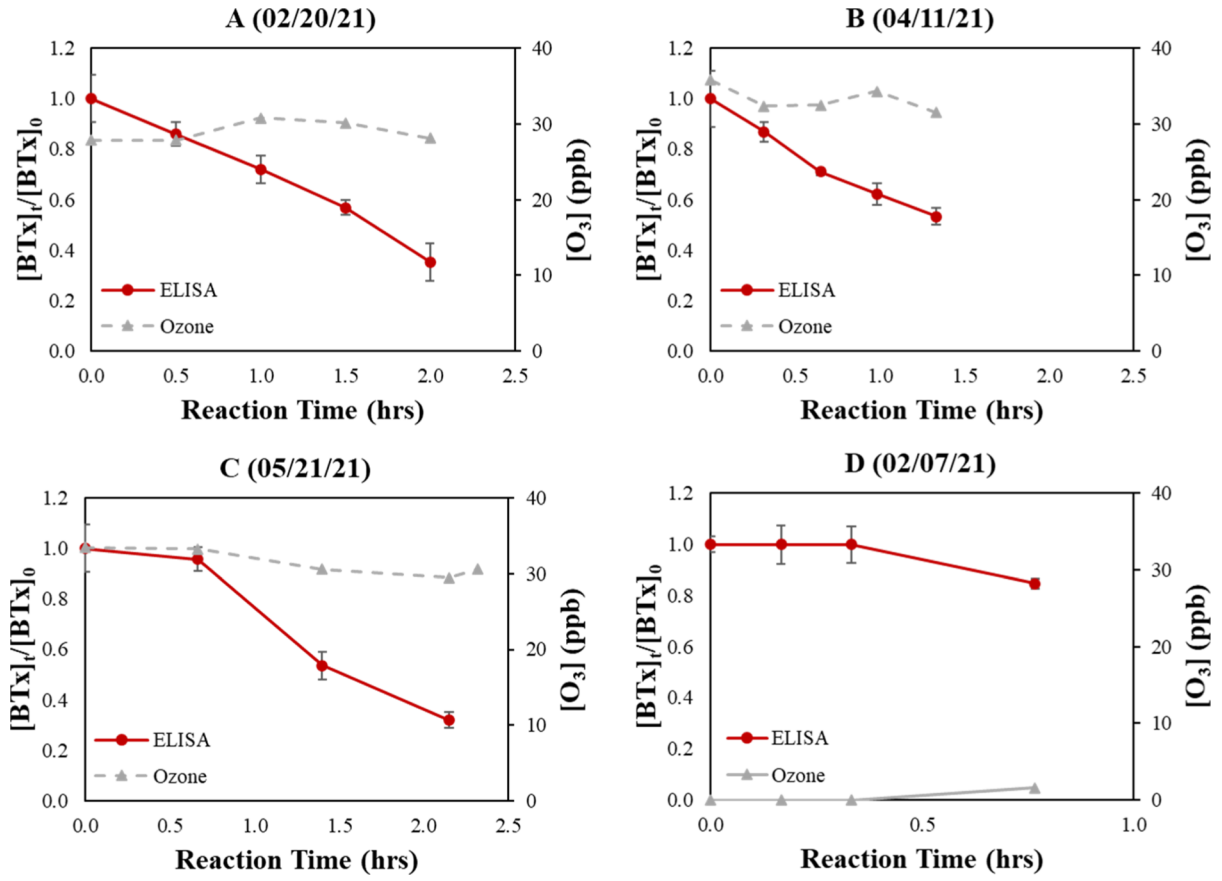

Figure 3. Degradation of BTx in chamber-generated SSA in the presence of O_3. Each point represents the average of triplicate measurements taken with competitive ELISA. Error bars represent the standard error for the mean BTx concentration at each time point when α = 0.95.

Access triple quadrupole MS/MS (Thermo Fisher Scientific, Waltham, MA). The analytical column was a Kinetex 2.6 μm particle size (Phenomenex, Torrance, CA) with dimensions of 100 × 2.1 mm. The solvent gradient was composed of acetonitrile with 0.1% formic acid (A) and HPLC water with 0.1% formic acid (B) with initial conditions of 50:50 (A/B) for 10 min to 95:5 for 5 min and a holdback to 50:50 for 5 min for a total sample run time of 20 min at a flow rate of 200 μL/min.

RESULTS AND DISCUSSION

Distribution of BTx in Different Phases of SSA. SSA is composed of inorganic salts and OM, which are immiscible and form two different phases within aerosols below 90−92% RH.[24,25] As RH decreases, the salt concentration in SSA increases.[30] Knowledge of the distribution of BTx across these two phases is fundamental for the characterization of its degradation kinetics, as reaction rates may be impacted by the uptake of oxidants into each phase and their interactions with surrounding compounds. The Hansen group's contribution method[27] and the AIOMFAC inorganic thermodynamic model[28] were used to determine the distribution of BTx among the phases of SSA. Using Hansen's method, the estimated activity coefficient of BTx in the OM of SSA ($\gamma_{BTx\text{-}3,OM}$) is 0.569, suggesting that BTx is highly soluble in this phase.[27] Using the AIOMFAC model, the estimated activity coefficient of the compound in the aqueous salt core of SSA ($\gamma_{BTx\text{-}3,aq}$) is 1.43 × 10^{19}, suggesting that BTx is insoluble in this phase.[28] The large difference in magnitude between these values indicates that BTx largely partitions to the organic layer. Thus, the reaction between BTx and atmospheric oxidants can be assumed to mainly occur within the OM of SSA.

BTx Decay under O_3 Exposure. Figure 3A−C shows that the exposure of BTx-containing SSA to O_3 alone results in a large decrease in BTx concentrations, as the decrease between successive measurements exceeds the standard error of the preceding measurement. O_3 is present at a stable concentration in the chamber at the time of the introduction of SSA, resulting in BTx decay occurring immediately after its nebulization into the chamber. In the absence of O_3 and sunlight, BTx concentrations do not change by an amount greater than the standard error (Figure 3D).

Ozonolysis of BTx can be expressed by the following second-order reaction

$$\frac{d[BTx]}{dt} = -k_{BTx,O_3}[O_3]_{OM}[BTx] \quad (1)$$

where $[O_3]_{OM}$ represents the concentration of O_3 dissolved in the OM of the aerosol, and [BTx] represents the concentration of BTx in the aerosol. As shown in Figure 3, the concentration of ozone in the chamber remained relatively constant throughout the entirety of each experiment. Thus, the ozonolysis of BTx can be assumed to occur through a pseudo-first-order reaction in which $[O_3]_{OM}$ has a constant value, while [BTx] varies throughout the course of the reaction. $[O_3]_{OM}$ is estimated by multiplying the measured gaseous O_3 concentration with the partitioning constant of O_3 onto OM (K_{P,O_3-OM} in mol/m^3·Pa).[31] Currently, few

https://doi.org/10.1021/acs.est.1c05740
Environ. Sci. Technol. 2022, 56, 1811−1819

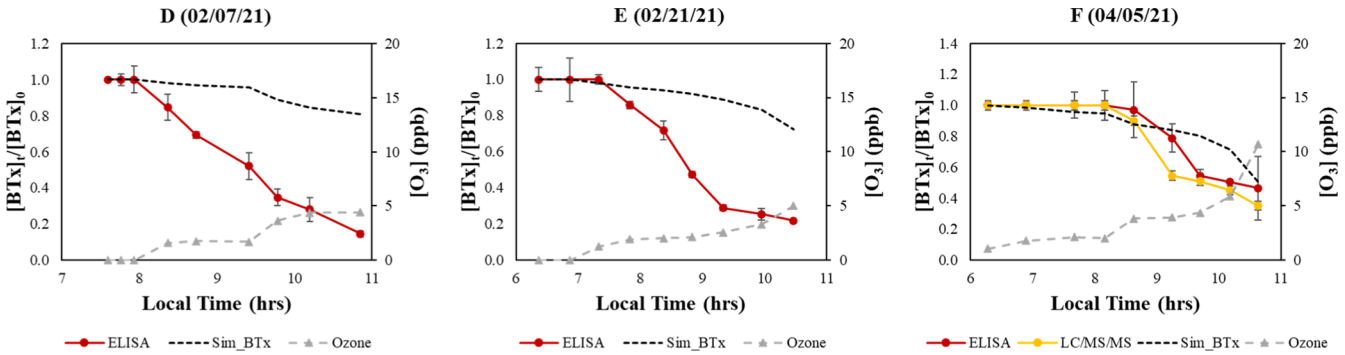

Figure 4. Degradation of BTx in chamber-generated SSA in the presence of sunlight. Each point represents the average of triplicate measurements taken with competitive ELISA. Error bars represent the standard error for the mean BTx concentration at each time point when $\alpha = 0.95$.

experimental values for the Henry's law constant of O_3 in organic solvents is available in the literature.[32] A 2014 IUPAC-NIST data series found that the solubility ($c_{1,liq}/c_{1/gas}$) of ozone in five different organic solvents at 273.15 K ranged from 1.5 to 2.0, on average 5.5 times higher than the solubility of ozone in water at the same temperature.[33] Using this ratio, K_{P,O_3-OM} can be estimated to be 7.11×10^{-3} mol/m^3 Pa.[31,33] From the above equation and assumptions, the average reaction rate constant of BTx ozonolysis (k_{BTx,O_3}) is $5.74 \pm 0.21 \times 10^3$ M^{-1} s^{-1} (Figure S2).

To identify the reactivity of potential functional groups of BTx with ozone, the theoretical rate constant for BTx ozonolysis was estimated using the quantitative structure−reactivity relationship (QSRR) method described by Atkinson and Carter in 1984.[34] O_3 reactions with organic compounds are mostly limited to reactions with alkenes, although some nitrogen functional groups in proteins can undergo the reaction with O_3.[35] Figure S3 illustrates the predicted reaction rate constants of three different alkene units in BTx-3 with ozone in gas phase. The functional group predicted to undergo reaction at the fastest rate with ozone is the *cis* unsaturated carbon−carbon bond on ring 8. In the body, BTx acts as a voltage-gated sodium channel activator through the binding of its polyether backbone to site 5 of the channel receptors.[36] The ozonolysis of the unsaturated carbon−carbon bonds within the backbone may lead to ring opening, affecting the binding of BTx to the receptors and modulating its perceived toxicity.[9,37]

BTx Decay under UV Exposure. Figure 4 shows the decay of BTx in SSA exposed to sunlight, with "ELISA" indicating the measured change in concentrations and "Sim_BTx" indicating the expected change in concentrations estimated by O_3 concentrations and the k_{BTx,O_3} value calculated above. The data from all four experiments in Figure 4 show a large difference between the measured decay and that predicted in "Sim_BTx," which increases as the aerosol ages. This discrepancy suggests that oxidants other than O_3 must contribute to the decay of BTx in the presence of sunlight. The difference between the BTx concentrations predicted by "Sim_BTx" and measured by ELISA for Experiments D and E and those for experiment F can be attributed to the differences in UV irradiation by each experiment (Figure S1). Due to the incidence of less UV radiation in experiment F, BTx decay occurs to a greater extent from ozonolysis, resulting in a smaller difference to the decay predicted by "Sim_BTx" than in the previous two experiments. LC/MS/MS generally has a higher accuracy of measurement than ELISA. The similar trend in $[BTx]_t/[BTx]_0$ measured by ELISA and LC/MS/MS during Experiment F indicates that ELISA can measure BTx concentrations to a similar degree of accuracy as high-performance analytical instruments.

In the morning, OH radicals are produced under sunlight from the photolysis of chemical species present in ambient air at trace concentrations, such as HONO, HC(O)H, $CH_3(O)H$, and H_2O_2.[38] In the chamber, HONO is heterogeneously produced from reactions with the chamber walls. Trace concentrations of HC(O)H, $CH_3(O)H$, and H_2O_2 are present in the chamber from slight intrusion of ambient air over the course of the experiments (2.6% change). In addition to photolysis, these species can form OH radicals through photochemical reactions in the presence of NO_x, which is present at less than 3 ppb in the chamber and 25−35 ppb in coastal Southwest Florida.[38,39] During daytime conditions, photolysis of O_3 produced from these photochemical reactions with NO_x and hydrocarbons is the major source of OH radicals.[38] Additionally, OH radicals formed from the photolysis of O_3 can react with Cl^- ions in SSA to form HOCl.[40] Dissociation of HOCl in the process of chlorine offgassing from the SSA results in the formation of Cl and OH radicals, which can further contribute to the photochemical oxidation of BTx.[40] The potential reactivity of functional units in BTx with OH radicals was evaluated by using the rate constant in the gaseous phase, which was predicted by the quantitative structure−reactivity relationship method (QSRR) described by Kwok and Atkinson in 1995.[41] Figure S4 shows the estimated reaction rate constants of BTx-3 functional groups with OH radicals using this method. OH radicals can react with more functional groups in BTx than O_3, such as through H-atom abstraction from aliphatic C−H and O−H bonds or through radical addition to olefinic groups or aromatic rings.[35] The reactions of the aliphatic groups in BTx with OH radicals are also of importance because alkoxy groups in ether linkages can increase their reactivity (Figure S4). Based on this structure−reactivity relationship, the three carbon−carbon double bonds contribute to 26% and the tertiary aliphatic carbons with alkoxy substituents contribute to 68% of BTx reactions with OH radicals. OH radical addition to the unsaturated C−H bonds and OH abstraction of C−H bonds can result in ring opening and the formation of oxygenated derivatives, resulting in modulation of the compound's toxic effects.[9,37]

Effects of OM on BTx Decay. Previous studies on the photodegradation of BTx in seawater suggest that their decay in the presence of sunlight is increased by the presence of OM.[13,14,42] Highly conjugated organic compounds ubiqui-

https://doi.org/10.1021/acs.est.1c05740
Environ. Sci. Technol. 2022, 56, 1811−1819

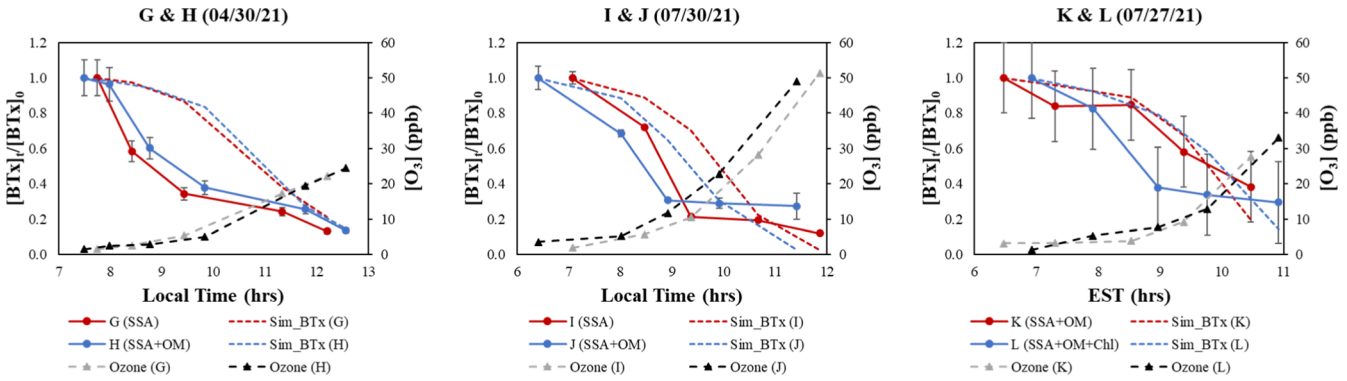

Figure 5. Change in BTx concentrations in SSA in the presence and absence of OM upon exposure to sunlight. Each point represents the average of triplicate measurements taken with competitive ELISA. Error bars represent the standard error for the mean BTx concentration at each time point when $\alpha = 0.95$.

tously found in seawater, such as chlorophyll and humic compounds, can absorb sunlight and enter an excited state.[13] Transfer of energy from the excited compound to triplet oxygen results in the formation of singlet oxygen or reactive radicals (i.e., hydroxyl, peroxy, and alkoxy radicals), which then contribute to the further degradation of BTx.[13,14]

The *K. brevis* solution was obtained from bulk seawater, which has a much smaller OM fraction than the surface microlayer from which SSA are usually generated. Spikes of non-photosensitizing (proteins, polysaccharides, and lipids) and photosensitizing (chlorophyll) OM were added to the solution to understand the impact of co-existing OM on BTx degradation. The impact of OM on BTx ozonolysis was negligible, as the reaction rate constant of BTx ozonolysis in the presence of OM ($k_{BTx,O_3-OM} = 5.96 \pm 0.22 \times 10^3\ M^{-1}\ s^{-1}$, Figure S2c) was insignificantly different from that found in the absence of OM ($k_{BTx,O_3} = 5.74 \pm 0.21 \times 10^3\ M^{-1}\ s^{-1}$, Figure S2a,b). Some functional groups in OM found in SSA can react with O_3, such as olefinic side groups in amino acids or alkenes in long fatty acid chains.[43] Ozonolysis can also form hydroxyl or alkyl radicals, which can further oxidize algal OM. The insignificant difference between the k_{BTx,O_3} values in the presence and absence of OM indicates that BTx decay through ozonolysis occurs through direct reaction with O_3.

In Experiments G-J, BTx decay in the absence and presence of non-photosensitizing OM (Figure 5) occurs at a similar rate, as the BTx concentration at each time point of one condition is within the standard error of its counterpart in the other condition. BTx in SSA containing 24 wt % OM appears to degrade at a slightly slower rate than BTx in SSA with a much smaller OM fraction (0.7 wt %). In Experiment H, SSA with non-photosensitizing OM are aged within the west UF-APHOR chamber, while in Experiment J, SSA with non-photosensitizing OM are aged within the east UF-APHOR chamber. The east chamber receives slightly greater UV irradiation than the west chamber throughout the morning. Thus, the delay in the rate of BTx decay observed in SSA with added non-photosensitizing matter can be attributed to its aerosol characteristics instead of its chamber location. Unlike ozone, the OH radical produced in daytime is less selective and reacts with various organic species on the surface of SSA. The slight deceleration of BTx decay in the presence of non-photosensitizing OM suggests that it can compete with BTx for heterogeneous reactions with OH radicals to a very small extent.

In addition to changes in BTx concentrations, the composition of SSA dynamically changes under sunlight. For example, Figure S5 shows the change in chemical composition within the inorganic salt phase of SSA. Oxidation of OM in SSA forms carboxylic acids. Alkaline cations, mainly comprising sodium ions, can interact with these carboxylic acids to form carboxylate salts, resulting in the depletion of chloride ion from SSA through the release of gaseous HCl.[44−46] The greater decrease in the Na/Cl molar concentration of SSA with a large OM fraction relative to that with a small OM fraction under sunlight suggests that faster degassing of Cl from SSA occurs due to the aging of OM.[47]

Experiments K and L examine the degradation of BTx in the presence of chlorophyll, a photosensitizing compound abundant in seawater (Figure 5). The small difference in $[BTx]_t/[BTx]_0$ ratios between the two chamber conditions indicates that the photosensitization of chromophores apparently does not contribute to BTx degradation in SSA, unlike conditions observed in seawater.

Figure S6 depicts the UV spectra of chlorophyll *a*-containing cyanobacteria at various times of the day. The gradual decrease of the absorbance peaks at 450 and 680 nm from early morning to early afternoon indicates that chlorophyll *a* undergoes degradation in the presence of sunlight.[48,49] Upon the depletion of these chromophores, the photosensitization mechanism of degradation cannot occur. In a similar manner, other humic-like chromophores can be bleached under sunlight.

Atmospheric Implications and Uncertainties. Between late afternoon and midnight, O_3 is the dominant oxidant present in the atmosphere. During these times in the summer, wind blows inland due to sea surface temperatures remaining lower than land surface temperatures. Along the Florida Gulf Coast during the red tide season (July−October), suburban areas have average O_3 concentrations of 20 ppb, while urban areas have average O_3 concentrations of 50 ppb.[50,51] Additionally, during this season the average nightfall wind speed is 5 knots (9.26 km/h) and the average nightfall temperature is approximately 21 °C.[52] Using these meteorological values and the BTx ozonolysis rate constant ($k_{BTx,O_3} = 5.74 \pm 0.21 \times 10^3\ M^{-1}\ s^{-1}$), the atmospheric lifetime of BTx in nighttime conditions for 87.5% decay (three half-lives) of BTx without dispersion is 7.08 ± 0.26 h in suburban areas and 2.83 ± 0.10 h in urban areas. In applying a Gaussian dispersion model to predict the transport of aerosolized BTx from red tide

https://doi.org/10.1021/acs.est.1c05740
Environ. Sci. Technol. 2022, 56, 1811−1819

events, dispersion can be assumed to occur mainly in the vertical direction due to the formation of aerosols from a line source.[53] During clear nighttime conditions in urban areas, 85% of aerosolized BTx undergoes dispersion within approximately 2 km from the bloom. Using the lifetime estimated above, an additional 15% of remaining BTx undergoes decay via ozonolysis within this distance in urban areas.

During daytime conditions, aerosolized BTx undergoes greater reduction in concentrations because of greater degradation under sunlight (Figure 4) and greater dispersion. A single red tide bloom lasts an average of 6 weeks in the Gulf of Mexico, and UV irradiation or cloud cover can vary greatly between days during this period.[54] With more extensive cloud cover, greater inland transport of BTx before degradation by sunlight can occur.

The conditions of the chamber experiments conducted in this study do not fully represent real-life conditions in which aerosolized BTx is found. The OM fraction used in this study consists of proxy compounds that were chosen to represent functional groups commonly identified in aerosolized OM, as the specific organic compounds found in SSA have not yet been widely identified.[26] Though they share similar structural features, the OM fraction used here is "inauthentic" and may not wholly encapsulate natural processes found in naturally occurring SSA. Additionally, the Florida Gulf Coast contains several heavily populated areas with high daytime NO_x and hydrocarbon concentrations, which may serve as a source of oxidants, which can undergo reactions with BTx in SSA. Such reactions are not accounted for in this study, which focuses on only two major atmospheric oxidants. Studies on BTx decay in SSA collected *in situ* along coastal areas during various times of the day can allow for a more accurate characterization of BTx degradation under environmental conditions.

Additionally, the ELISA employed in this study is mainly sensitive to BTx variants with a BTx B structural backbone, namely, BTx-2 and BTx-3. These two variants naturally occur the most outside of the cell, so the reaction rate constant calculated based on ELISA measurements can be considered a fair approximation of actual atmospheric processes.[10,11] However, uncertainty in the rate constants' validity remains due to their lack of accounting for the decay of variants with a BTx A structural backbone, such as BTx-1. The use of multiple ELISAs measuring both BTx A and BTx B variants will allow for a more accurate characterization of BTx atmospheric processes.

Furthermore, the degradation of BTx does not necessarily result in the reduction of toxicity. Derivatives formed from BTx oxidation in SSA can have widely varying functionalities, ranging from increased toxicity to antagonistic behavior toward BTx.[9] The travel distances stated earlier may not reflect the full geographic range in which BTx can cause adverse health effects. Toxicology studies characterizing the functions of these oxidation products would allow for an increased understanding of the hazards of aerosolized BTx after atmospheric aging.

■ ASSOCIATED CONTENT

Supporting Information

The Supporting Information is available free of charge at https://pubs.acs.org/doi/10.1021/acs.est.1c05740.

Time profiles of temperature, RH, and sunlight for outdoor chamber experiments; determination of reaction rate constant for BTx ozonolysis; contributing groups to structural reactivity of BTx-3 with O_3 and OH radicals; change in chlorine/sodium concentration ratios in SSA during photochemical aging; and UV spectra of chlorophyll *a* in SSA at various stages of photochemical aging (PDF)

■ AUTHOR INFORMATION

Corresponding Author

Myoseon Jang − *Department of Environmental Engineering Sciences, University of Florida, Gainesville, Florida 32611, United States;* orcid.org/0000-0003-4211-7883; Email: mjang@ufl.edu

Authors

Karen Sem − *Department of Environmental Engineering Sciences, University of Florida, Gainesville, Florida 32611, United States*

Richard Pierce − *Mote Marine Laboratory, Sarasota, Florida 34326, United States*

Patricia Blum − *Mote Marine Laboratory, Sarasota, Florida 34326, United States*

Zechen Yu − *Department of Environmental Engineering Sciences, University of Florida, Gainesville, Florida 32611, United States;* orcid.org/0000-0002-6763-0520

Complete contact information is available at: https://pubs.acs.org/10.1021/acs.est.1c05740

Notes

The authors declare no competing financial interest.

■ ACKNOWLEDGMENTS

This work was supported by grants from the Florida Fish and Wildlife Conservation Commission (PO # B7E13E) and from the National Science Foundation (AGS 1923651 and AGS 2044921).

■ REFERENCES

(1) Anderson, D. M.; Fensin, E.; Gobler, C. J.; Hoeglund, A. E.; Hubbard, K. A.; Kulis, D. M.; Landsberg, J. H.; Lefebvre, K. A.; Provoost, P.; Richlen, M. L.; Smith, J. L.; Solow, A. R.; Trainer, V. L. Marine Harmful Algal Blooms (HABs) in the United States: History, Current Status and Future Trends. *Harmful Algae* **2021**, *102*, 101975.

(2) Pierce, R. H.; Henry, M. S.; Blum, P. C.; Lyons, J.; Cheng, Y. S.; Yazzie, D.; Zhou, Y. Brevetoxin Concentrations in Marine Aerosol: Human Exposure Levels During a Karenia Brevis Harmful Algal Bloom. *Bull. Environ. Contam. Toxicol.* **2003**, *70*, 161−165.

(3) Gawley, R. E.; Rein, K. S.; Jeglitsch, G.; Adams, D. J.; Theodorakis, E. A.; Tiebes, J.; Nicolaou, K. C.; Baden, D. G. The Relationship of Brevetoxin 'Length' and A-Ring Functionality to Binding and Activity in Neuronal Sodium Channels. *Chem. Biol.* **1995**, *2*, 533−541.

(4) Hilderbrand, S. C.; Murrell, R. N.; Gibson, J. E.; Brown, J. M. Marine Brevetoxin Induces IgE-Independent Mast Cell Activation. *Arch. Toxicol.* **2011**, *85*, 135−141.

(5) Abraham, W. M.; Bourdelais, A. J.; Sabater, J. R.; Ahmed, A.; Lee, T. A.; Serebriakov, I.; Baden, D. G. Airway Responses to Aerosolized Brevetoxins in an Animal Model of Asthma. *Am. J. Respir. Crit. Care Med.* **2005**, *171*, 26−34.

(6) Cheng, Y. S.; McDonald, J. D.; Kracko, D.; Irvin, C. M.; Zhou, Y.; Pierce, R. H.; Henry, M. S.; Bourdelaisa, A.; Naar, J.; Baden, D. G. Concentration and Particle Size of Airborne Toxic Algae (Brevetoxin) Derived from Ocean Red Tide Events. *Environ. Sci. Technol.* **2005**, *39*, 3443−3449.

(7) Pierce, R. H.; Henry, M. S.; Blum, P. C.; Hamel, S. L.; Kirkpatrick, B.; Cheng, Y. S.; Zhou, Y.; Irvin, C. M.; Naar, J.; Weidner, A.; Fleming, L. E.; Backer, L. C.; Baden, D. G. Brevetoxin Composition in Water and Marine Aerosol along a Florida Beach: Assessing Potential Human Exposure to Marine Biotoxins. *Harmful Algae* **2005**, *4*, 965−972.
(8) Hoagland, P.; Jin, D.; Polansky, L. Y.; Kirkpatrick, B.; Kirkpatrick, G.; Fleming, L. E.; Reich, A.; Watkins, S. M.; Ullmann, S. G.; Backer, L. C. The Costs of Respiratory Illnesses Arising from Florida Gulf Coast Karenia Brevis Blooms. *Environ. Health Perspect.* **2009**, *117*, 1239−1243.
(9) Baden, D. G.; Bourdelais, A. J.; Jacocks, H.; Michelliza, S.; Naar, J. Natural and Derivative Brevetoxins: Historical Background, Multiplicity, and Effects. *Environ. Health Perspect.* **2005**, *113*, 621−625.
(10) Errera, R. M.; Bourdelais, A.; Drennan, M. A.; Dodd, E. B.; Henrichs, D. W.; Campbell, L. Variation in Brevetoxin and Brevenal Content among Clonal Cultures of Karenia Brevis May Influence Bloom Toxicity. *Toxicon* **2010**, *55*, 195−203.
(11) Pierce, R.; Henry, M.; Blum, P. Brevetoxin Abundance and Composition during ECOHAB-Florida Field Monitoring Cruises in the Gulf of Mexico. *Cont. Shelf Res.* **2008**, *28*, 45−58.
(12) Abraham, A.; El Said, K. R.; Wang, Y.; Jester, E. L. E.; Plakas, S. M.; Flewelling, L. J.; Henry, M. S.; Pierce, R. H. Biomarkers of Brevetoxin Exposure and Composite Toxin Levels in Hard Clam (Mercenaria Sp.) Exposed to Karenia Brevis Blooms. *Toxicon* **2015**, *96*, 82−88.
(13) Hardman, R. C.; Cooper, W. J.; Bourdelais, A. J.; Gardinali, P.; Baden, D. G. Brevetoxin Degradation and By-Product Formation via Natural Sunlight. *Harmful Algae 2002 Proc. Xth Int. Conf. Harmful Algae St Pete Beach Fla. USA Oct. 21−25 2002*; 2004; Vol. *10*, pp 153−154.
(14) Kieber, R. J.; Pitt, J.; Skrabal, S. A.; Wright, J. L. C. Photodegradation of the Brevetoxin PbTx-2 in Coastal Seawater. *Limnol. Oceanogr.* **2010**, *55*, 2299−2304.
(15) Schneider, K. R.; Pierce, R. H.; Rodrick, G. E. The Degradation of Karenia Brevis Toxins Utilizing Ozonated Seawater. *Harmful Algae* **2003**, *2*, 101−107.
(16) Jang, M.; Berthold, D. E.; Yu, Z.; Silva-Sanchez, C.; Laughinghouse, H. D.; Denslow, N. D.; Han, S. Atmospheric Progression of Microcystin-LR from Cyanobacterial Aerosols. *Environ. Sci. Technol. Lett.* **2020**, *7*, 740−745.
(17) Wang, X.; Deane, G. B.; Moore, K. A.; Ryder, O. S.; Stokes, M. D.; Beall, C. M.; Collins, D. B.; Santander, M. V.; Burrows, S. M.; Sultana, C. M.; Prather, K. A. The Role of Jet and Film Drops in Controlling the Mixing State of Submicron Sea Spray Aerosol Particles. *Proc. Natl. Acad. Sci.* **2017**, *114*, 6978−6983.
(18) Jayarathne, T.; Sultana, C. M.; Lee, C.; Malfatti, F.; Cox, J. L.; Pendergraft, M. A.; Moore, K. A.; Azam, F.; Tivanski, A. V.; Cappa, C. D.; Bertram, T. H.; Grassian, V. H.; Prather, K. A.; Stone, E. A. Enrichment of Saccharides and Divalent Cations in Sea Spray Aerosol During Two Phytoplankton Blooms. *Environ. Sci. Technol.* **2016**, *50*, 11511−11520.
(19) Ault, A. P.; Moffet, R. C.; Baltrusaitis, J.; Collins, D. B.; Ruppel, M. J.; Cuadra-Rodriguez, L. A.; Zhao, D.; Guasco, T. L.; Ebben, C. J.; Geiger, F. M.; Bertram, T. H.; Prather, K. A.; Grassian, V. H. Size-Dependent Changes in Sea Spray Aerosol Composition and Properties with Different Seawater Conditions. *Environ. Sci. Technol.* **2013**, *47*, 5603−5612.
(20) Patterson, J. P.; Collins, D. B.; Michaud, J. M.; Axson, J. L.; Sultana, C. M.; Moser, T.; Dommer, A. C.; Conner, J.; Grassian, V. H.; Stokes, M. D.; Deane, G. B.; Evans, J. E.; Burkart, M. D.; Prather, K. A.; Gianneschi, N. C. Sea Spray Aerosol Structure and Composition Using Cryogenic Transmission Electron Microscopy. *ACS Cent. Sci.* **2016**, *2*, 40−47.
(21) Bertram, T. H.; Cochran, R. E.; Grassian, V. H.; Stone, E. A. Sea Spray Aerosol Chemical Composition: Elemental and Molecular Mimics for Laboratory Studies of Heterogeneous and Multiphase Reactions. *Chem. Soc. Rev.* **2018**, *47*, 2374−2400.
(22) Tang, I. N.; Tridico, A. C.; Fung, K. H. Thermodynamic and Optical Properties of Sea Salt Aerosols. *J. Geophys. Res. Atmos.* **1997**, *102*, 23269−23275.
(23) Gupta, D.; Eom, H.-J.; Cho, H.-R.; Ro, C.-U. Hygroscopic Behavior of NaCl−MgCl2 Mixture Particles as Nascent Sea-Spray Aerosol Surrogates and Observation of Efflorescence during Humidification. *Atmos. Chem. Phys.* **2015**, *15*, 11273−11290.
(24) Ciobanu, V. G.; Marcolli, C.; Krieger, U. K.; Weers, U.; Peter, T. Liquid−Liquid Phase Separation in Mixed Organic/Inorganic Aerosol Particles. *J. Phys. Chem. A* **2009**, *113*, 10966−10978.
(25) O'Brien, R. E.; Wang, B.; Kelly, S. T.; Lundt, N.; You, Y.; Bertram, A. K.; Leone, S. R.; Laskin, A.; Gilles, M. K. Liquid−Liquid Phase Separation in Aerosol Particles: Imaging at the Nanometer Scale. *Environ. Sci. Technol.* **2015**, *49*, 4995−5002.
(26) Cravigan, L. T.; Mallet, M. D.; Vaattovaara, P.; Harvey, M. J.; Law, C. S.; Modini, R. L.; Russell, L. M.; Stelcer, E.; Cohen, D. D.; Olsen, G.; Safi, K.; Burrell, T. J.; Ristovski, Z. Sea Spray Aerosol Organic Enrichment, Water Uptake and Surface Tension Effects. *Atmos. Chem. Phys.* **2020**, *20*, 7955−7977.
(27) Hansen, C. M. Theory—The Prigogine Corresponding States Theory, the X12 Interaction Parameter, and the Hansen Solubility Parameters. *Hansen Solubility Parameters: A User's Handbook*; CRC Press: Boca Raton, 2000; pp 67−83.
(28) Zuend, A.; Marcolli, C.; Booth, A. M.; Lienhard, D. M.; Soonsin, V.; Krieger, U. K.; Topping, D. O.; McFiggans, G.; Peter, T.; Seinfeld, J. H. New and Extended Parameterization of the Thermodynamic Model AIOMFAC: Calculation of Activity Coefficients for Organic-Inorganic Mixtures Containing Carboxyl, Hydroxyl, Carbonyl, Ether, Ester, Alkenyl, Alkyl, and Aromatic Functional Groups. *Atmos. Chem. Phys.* **2011**, *11*, 9155−9206.
(29) Beardsley, R.; Jang, M.; Ori, B.; Im, Y.; Delcomyn, C. A.; Witherspoon, N. Role of Sea Salt Aerosols in the Formation of Aromatic Secondary Organic Aerosol: Yields and Hygroscopic Properties. *Environ. Chem.* **2013**, *10*, 167.
(30) Freedman, M. A. Liquid−Liquid Phase Separation in Supermicrometer and Submicrometer Aerosol Particles. *Acc. Chem. Res.* **2020**, *53*, 1102−1110.
(31) Sander, R. Compilation of Henry's Law Constants (Version 4.0) for Water as Solvent. *Atmos. Chem. Phys.* **2015**, *15*, 4399−4981.
(32) Battino, R.; Rettich, T. R.; Tominaga, T. The Solubility of Oxygen and Ozone in Liquids. *J. Phys. Chem. Ref. Data* **1983**, *12*, 163−178.
(33) Miyamoto, H.; Yampolski, Y.; Young, C. L. IUPAC-NIST Solubility Data Series. 103. Oxygen and Ozone in Water, Aqueous Solutions, and Organic Liquids (Supplement to Solubility Data Series Volume 7). *J. Phys. Chem. Ref. Data* **2014**, *43*, 033102.
(34) Atkinson, R.; Carter, W. P. L. Kinetics and Mechanisms of the Gas-Phase Reactions of Ozone with Organic Compounds under Atmospheric Conditions. *Chem. Rev.* **1984**, *84*, 437−470.
(35) Atkinson, R. Atmospheric Oxidation. In *Handbook of Property Estimation Methods for Chemicals: Environmental and Health Sciences*; Boethling, R. S., Mackay, D., Eds.; Lewis Publishers: Boca Raton, 2000; pp 358−377.
(36) Jeglitsch, G.; Rein, K.; Baden, D. G.; Adams, D. J. Brevetoxin-3 (PbTx-3) and Its Derivatives Modulate Single Tetrodotoxin-Sensitive Sodium Channels in Rat Sensory Neurons. *J. Pharmacol. Exp. Ther.* **1998**, *284*, 516−525.
(37) Hua, Y.; Cole, R. B. Solution Reactivity of Brevetoxins As Monitored by Electrospray Ionization Mass Spectrometry and Implications for Detoxification. *Chem. Res. Toxicol.* **1999**, *12*, 1268−1277.
(38) Finlayson-Pitts, B. J.; Pitts, J. N. Rates and Mechanisms of Gas-Phase Reactions in Irradiated Organic-NOx-Air Mixtures. *Chemistry of the Upper and Lower Atmosphere: Theory, Experiments, and Applications*; Academic Press: San Diego, 2000; pp 179−263.
(39) Walsh, H. *2020 Design Values for Nitrogen Dioxide*; Florida Department of Environmental Protection, 2021.
(40) Oum, K. W.; Lakin, M. J.; DeHaan, D. O.; Brauers, T.; Finlayson-Pitts, B. J. Formation of Molecular Chlorine from the

https://doi.org/10.1021/acs.est.1c05740
Environ. Sci. Technol. 2022, 56, 1811−1819

Photolysis of Ozone and Aqueous Sea-Salt Particles. *Science* **1998**, *279*, 74−76.
(41) Kwok, E.; Atkinson, R. Estimation of Hydroxyl Radical Reaction Rate Constants for Gas-Phase Organic Compounds Using a Structure-Reactivity Relationship: An Update. *Atmos. Environ.* **1995**, *29*, 1685−1695.
(42) Khan, U.; Benabderrazik, N.; Bourdelais, A. J.; Baden, D. G.; Rein, K.; Gardinali, P. R.; Arroyo, L.; O'Shea, K. E. UV and Solar TiO2 Photocatalysis of Brevetoxins (PbTxs). *Toxicon* **2010**, *55*, 1008−1016.
(43) Atkinson, R.; Aschmann, S. M. Hydroxyl Radical Production from the Gas-Phase Reactions of Ozone with a Series of Alkenes under Atmospheric Conditions. *Environ. Sci. Technol.* **1993**, *27*, 1357−1363.
(44) Laskin, A.; Moffet, R. C.; Gilles, M. K.; Fast, J. D.; Zaveri, R. A.; Wang, B.; Nigge, P.; Shutthanandan, J. Tropospheric Chemistry of Internally Mixed Sea Salt and Organic Particles: Surprising Reactivity of NaCl with Weak Organic Acids: Mixed Sea Salt/Organics Particles. *J. Geophys. Res. Atmos.* **2012**, *117*, D15302.
(45) Bondy, A. L.; Wang, B.; Laskin, A.; Craig, R. L.; Nhliziyo, M. V.; Bertman, S. B.; Pratt, K. A.; Shepson, P. B.; Ault, A. P. Inland Sea Spray Aerosol Transport and Incomplete Chloride Depletion: Varying Degrees of Reactive Processing Observed during SOAS. *Environ. Sci. Technol.* **2017**, *51*, 9533−9542.
(46) Hossaini, R.; Chipperfield, M. P.; Saiz-Lopez, A.; Fernandez, R.; Monks, S.; Feng, W.; Brauer, P.; von Glasow, R. A Global Model of Tropospheric Chlorine Chemistry: Organic versus Inorganic Sources and Impact on Methane Oxidation: Model of Tropospheric Cl Chemistry. *J. Geophys. Res. Atmos.* **2016**, *121*, 14,271−14,297.
(47) Lee, A. K. Y.; Herckes, P.; Leaitch, W. R.; Macdonald, A. M.; Abbatt, J. P. D. Aqueous OH Oxidation of Ambient Organic Aerosol and Cloud Water Organics: Formation of Highly Oxidized Products: Aqueous Oxidation of Ambient Organics. *Geophys. Res. Lett.* **2011**, *38*, L11805.
(48) Shipman, L. L.; Cotton, T. M.; Norris, J. R.; Katz, J. J. An Analysis of the Visible Absorption Spectrum of Chlorophyll a Monomer, Dimer, and Oligomers in Solution. *J. Am. Chem. Soc.* **1976**, *98*, 8222−8230.
(49) Mackinney, G. Absorption of light by chlorophyll solutions. *J. Biol. Chem.* **1941**, *140*, 315−322.
(50) *Air Quality Monitoring*; Florida Department of Environmental Protection: Lido Park, 2021, July 26, 2021, AQS #L115-1005.
(51) *Air Quality Monitoring*; Florida Department of Environmental Protection: Jackson Road, Sarasota County, 2021, July 26, 2021, AQS #L115-2002.
(52) Station VENF1. *Historical Data & Climactic Summaries*; National Data Buoy Center, National Oceanic and Atmospheric Administration: Venice, FL, 2021, June 1, 2021.
(53) Turner, D. B. Estimates of Atmospheric Dispersion. *Workbook of Atmospheric Dispersion Estimates: an Introduction to Dispersion Modeling*; Lewis Publishers: Boca Raton, 1994; pp 22−70.
(54) Tominack, S. A.; Coffey, K. Z.; Yoskowitz, D.; Sutton, G.; Wetz, M. S. An Assessment of Trends in the Frequency and Duration of Karenia Brevis Red Tide Blooms on the South Texas Coast (Western Gulf of Mexico). *PLoS One* **2020**, *15*, No. e0239309.

https://doi.org/10.1021/acs.est.1c05740
Environ. Sci. Technol. 2022, 56, 1811−1819